RSC Advances

PAPER

View Article Online
View Journal | View Issue

Cite this: *RSC Adv.*, 2022, **12**, 13932

Highly dispersed ruthenium nanoparticles on nitrogen doped carbon toward efficient hydrogen evolution in both alkaline and acidic electrolytes†

Gen Li, Rui Gao, Zhongyu Qiu, Wei Liu and Yujiang Song *

Efficient and inexpensive electrocatalysts toward the hydrogen evolution reaction (HER) play an important role in electrochemical water splitting. Herein, we report the synthesis of highly dispersed ruthenium nanoparticles (2.2 ± 0.4 nm) on nitrogen doped carbon (Ru/N-C) by chemical reduction of $RuCl_3$ on carbon in the presence of polyvinylpyrrolidone in combination with subsequent pyrolysis. Ru/N-C exhibits an excellent overpotential of 13.5 and 18.5 mV at 10 mA cm^{-2} in 1.0 M KOH and 0.5 M H_2SO_4 aqueous solution, respectively, much better than and comparable to those of commercial Pt/C (38.0 and 10.0 mV). The exceptional HER activity arises from high surface area of ultrafine Ru nanoparticles and appropriate Ru electronic state tuned by nitrogen dopant. Furthermore, Ru/N-C demonstrates excellent durability in both alkaline and acidic condition relative to commercial Pt/C. We speculate that the nitrogen dopant might have coordinated with Ru and tightly anchored Ru nanoparticles, preventing them from agglomerating.

Received 27th April 2022
Accepted 1st May 2022

DOI: 10.1039/d2ra02671f

rsc.li/rsc-advances

Introduction

The dependence on carbon-based fossil fuels and intercorrelated environmental pollution urge us to develop renewable clean energy. Hydrogen is a unique energy carrier because of its zero-carbon merit. In contrast with steam methane reforming and coal gasification for hydrogen production, electrochemical water splitting is extremely attractive due to zero-CO_2 emission and the use of renewable electricity.[1] Besides anodic oxygen evolution reaction (OER), cathodic HER also needs highly efficient and inexpensive electrocatalysts for water splitting.[2,3] However, such advanced HER electrocatalysts remain as a challenge.[4]

Pt-based HER electrocatalysts are generally considered to be the best ones under both acidic and alkaline condition.[5] Unfortunately, the soaring cost and scarcity limit the employment of Pt. In order to circumvent this hurdle, great efforts have been devoted to low-cost and earth-abundant electrocatalysts including sulfides,[6–11] carbides,[12–14] nitrides,[12,13,15] phosphides[16–22] and phosphosulfides[23,24] as well as alloys.[25–27] However, the HER activity and durability are far inferior to that of Pt-based electrocatalysts.

Ru is the cheapest Pt group metals, whose price is only about 4% of Pt.[20,28] Meanwhile, Ru frequently exhibits attractive electrocatalytic performance similar to Pt.[3,29–34] These aspects indicate that Ru-based HER electrocatalysts might become an inexpensive alternative to Pt-based ones.

However, Ru is prone to agglomerate during synthesis and reaction owning to a large cohesive energy, diminishing its activity and durability.[35] Hence, the synthesis of highly dispersed and aggregation-resistant Ru-based HER electrocatalysts is required. In this regard, Ru/nitrogenated holey two-dimensional carbon structure (C_2N),[2] Ru/N-doped graphite carbon (NGC)[4] and hcp-Ru/N-C[36] have been reported. However, electrocatalysts with high HER performance under both alkaline and acidic conditions are very rare.[2]

Herein, we report the synthesis of highly dispersed Ru nanoparticles (NPs) loaded on nitrogen doped carbon through chemical reduction of $RuCl_3$ by ethylene glycol (EG) in the presence of polyvinylpyrrolidone (PVP) at 180 °C (Fig. 1 and S1†), followed by pyrolysis of adsorbed PVP at 350 °C to dope carbon support with N (Fig. S2†). The Ru and N content of resultant Ru/N-C is 15.1 wt% and 1.41 at%, respectively,

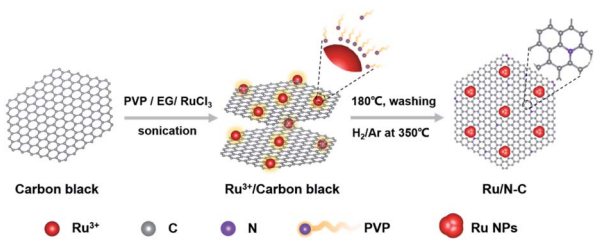

Fig. 1 Schematic diagram of the synthesis of Ru/N-C.

State Key Laboratory of Fine Chemicals, School of Chemical Engineering, Dalian University of Technology, 2 Linggong Road, Dalian 116024, China. E-mail: yjsong@dlut.edu.cn

† Electronic supplementary information (ESI) available. See https://doi.org/10.1039/d2ra02671f

according to thermogravimetric analysis (TGA, Fig. S3†) and X-ray photoelectron spectroscopy (XPS, Table S1†). For comparison, Pd/N-C, Ag/N-C, Ru/C, Pd/C, Ag/C were also synthesized under similar synthetic conditions (Fig. S4†).

Results and discussion

Transmission electron microscope (TEM) and high-angle annular dark-field scanning TEM (HAADF-STEM) reveal that Ru NPs are homogeneously distributed on nitrogen doped carbon with an average diameter of 2.2 ± 0.4 nm (Fig. 2a–c). Elemental mapping shows that Ru, N, and C are evenly dispersed in Ru/N-C (Fig. 2c). High resolution TEM (HRTEM) (Fig. 2d and e) and corresponding fast-Fourier transform pattern (FFT) (Fig. 2e, inset) show that Ru NPs are crystalline with a typical lattice spacing of 0.21 nm along (002) plane of hexagonal Ru. This was further corroborated by X-ray diffraction pattern (XRD) with the characteristic Ru (002) peak residing at 42.6° (Fig. 2f). The weak and broadened diffraction peak also indicates Ru exists in the form of fine NPs, consistent with the TEM results.

The C 1s XPS of Ru/N-C shows the peaks of C=O, C=N and C–C, locating at 289, 285.5 and 284.7 eV, respectively (Fig. 3a). In addition, the N 1s XPS of Ru/N-C (Fig. 3b) shows the subpeaks of oxidized-N, graphitic-N, pyrrolic-N and pyridinic-N at 403.1, 401, 400 and 398.3 eV, respectively. This again approves that nitrogen has been successfully doped into carbon by PVP pyrolysis.

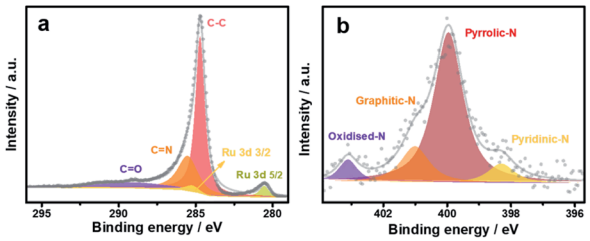

Fig. 3 (a) High-resolution XPS spectrum of C 1s + Ru 3d; (b) high-resolution XPS spectrum of N 1s.

Ru/N-C exhibits a small overpotential of 13.5 mV at 10 mA cm^{-2} toward HER in 1.0 M KOH aqueous solution (Fig. 4a and b), which is 24.5 mV lower than that of commercial Pt/C (38 mV). Ru/N-C also shows a higher turnover frequency (TOF) value of 0.56 H_2 per s per site at the overpotential of 25 mV than that of Pt/C (0.15 H_2 per s) as shown in Fig. S5a.† Moreover, the mass activity at the overpotential of 10 mV of Ru/N-C (353.3 mA mg_{Ru}^{-1}) is 4.9 times of Pt/C (72.3 mA mg_{Pt}^{-1}) in Fig. S5b.† The overpotential of Ru/C, Pd/N-C, Pd/C, Ag/N-C, Ag/C are all much larger than that of Ru/N-C (Fig. 4a and b). Especially, the overpotential of Ru/N-C is 36.5 mV lower than that of Ru/C (50 mV),

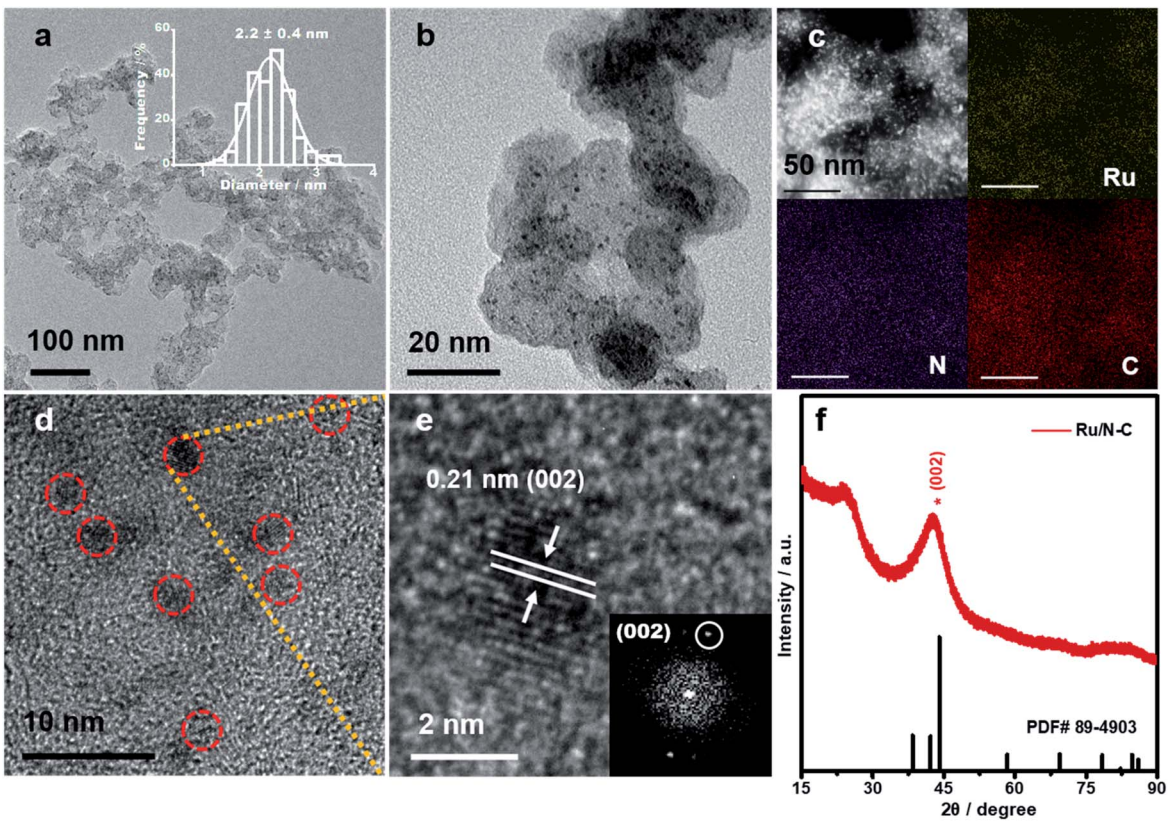

Fig. 2 (a) and (b) Typical TEM image of Ru/N-C at different magnifications. Inset: size distribution plotted by manually measuring at least 200 individual nanoparticles; (c) HAADF-STEM image of Ru/N-C and corresponding EDS mapping of ruthenium, nitrogen and carbon; (d and e) high-resolution TEM images of Ru/N-C. Insets: corresponding FFT; (f) XRD pattern of Ru/N-C.

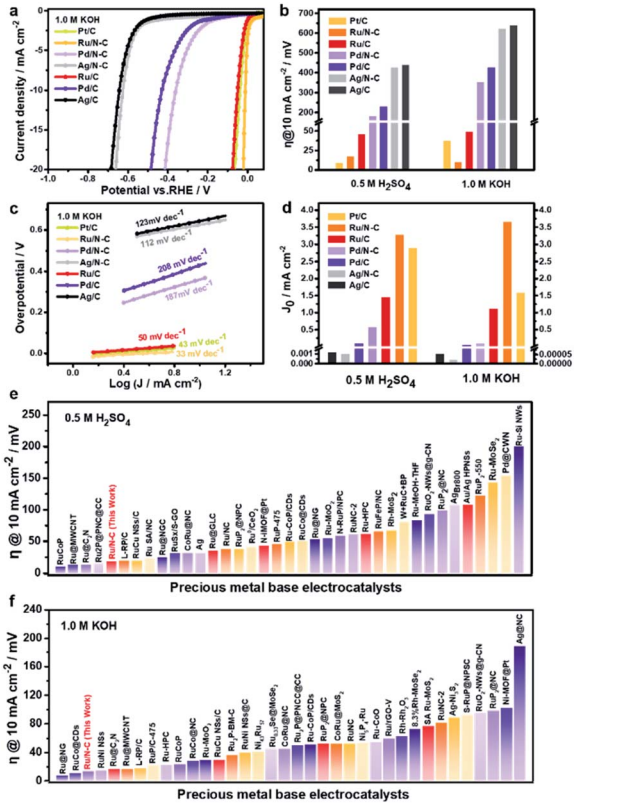

Fig. 4 (a) HER polarization curves recorded in N_2-saturated 1.0 M KOH aqueous solution; (b) overpotentials at 10 mA cm^{-2} collected in N_2-saturated 1.0 M KOH and 0.5 M H_2SO_4 aqueous solution; (c) Tafel plots in N_2-saturated 1.0 M KOH aqueous solution (d) exchange current density measured in N_2-saturated 1.0 M KOH and 0.5 M H_2SO_4 aqueous solution; comparison of the overpotentials at 10 mA cm^{-2} with documented noble metal based HER electrocatalysts in alkaline electrolytes (e) and acidic electrolytes (f).

which suggests that nitrogen doping is beneficial for the improvement of HER activity.

Furthermore, Ru/N-C possesses a Tafel slope of 33 mV dec^{-1} toward HER in 1.0 M KOH aqueous solution, suggestive of Volmer–Tafel HER mechanism (Fig. 4c).[37] In contrast, Ru/C shows a much larger Tafel slope of 50 mV dec^{-1} than that of Ru/N-C, indicative of Volmer–Heyrovsky HER mechanism.[37] With a low Tafel slope, the reaction rate of HER sharply rises with the overpotential, which is a competitive advantage for practical application. These results suggest that after N doping, the rate determined step (RDS) of HER has switched from Heyrovsky step to Tafel step, namely from electrochemical hydrogen desorption to chemical hydrogen desorption.[37] Meanwhile, the exchange current density (J_0) of Ru/N-C was determined to be 3.69 mA cm^{-2} by extrapolating the Tafel plot (Fig. 4d), which is more than twice that of commercial Pt/C (1.62 mA cm^{-2}). This suggests that Ru/N-C has a faster electron transfer rate and appropriate HER kinetics[29] relative to commercial Pt/C in alkaline electrolyte.

In 0.5 M H_2SO_4 aqueous solution, Ru/N-C also possesses a lower HER overpotential at 10 mA cm^{-2} (18.5 mV) than that of Ru/C, Pd/N-C, Pd/C, Ag/N-C, and Ag/C as shown in Fig. S6† and 4b. Especially, the overpotential of Ru/N-C toward acidic HER is only 8.5 mV higher than that of commercial Pt/C and the mass activity of Ru/N-C is 252.5 mA mg_{Ru}^{-1} which is slightly higher than that of Pt/C (248.3 mA mg_{Pt}^{-1}) (Fig. S7†). In addition, the Tafel slope of Ru/N-C is 36 mV dec^{-1} (Fig. S8†), which is the smallest among Ru/C, Pd/N-C, Pd/C, Ag/N-C, and Ag/C as well as comparable to that of commercial Pt/C (25 mV dec^{-1}). J_0 of Ru/N-C is 3.31 mA cm^{-2}, even higher than that of commercial Pt/C (2.93 mA cm^{-2}) as shown in Fig. 4d. Overall, Ru/N-C ranks at the top when compared with recently reported noble metal-based HER electrocatalysts in both acidic (Fig. 4e and Table S2†) and alkaline electrolytes (Fig. 4f and Table S3†).

For gaining more understanding on the origin of the excellent HER activity of Ru/N-C, high-resolution XPS of Ru 3p was performed (Fig. 5a). The two peaks residing at 484.5 and 462.1 eV, respectively, are assigned to metallic Ru $3p_{1/2}$ and Ru $3p_{3/2}$ of Ru/N-C, which positively shifts 0.6 eV relative to that of Ru/C. This suggests that Ru has donated electron to N dopant. In other words, the N-doped carbon support has significantly influenced the electronic structure of Ru, making Ru reach a favourable chemical state for HER.

In addition, the small diameter of Ru NPs (2.2 ± 0.4 nm) compared with other Ru NPs electrocatalysts[29,32–34,38] should be another reason for the excellent HER activity. Such well dispersed ultrafine particles expose a large number of Ru active sites unlike agglomerated ones. It is worth pointing out that the dispersity of Ru nanoparticle is sensitive to the pyrolysis temperature. A high pyrolysis temperature corresponds to a large particle size (Fig. S9 and S10†). It turned out that 350 °C is a good choice, at which nitrogen doping and the prevention of Ru NPs aggregation can simultaneously be realized (Fig. S11†). Moreover, a large surface area of support can offer more nucleation sites, allowing a more dispersive state and a smaller particle size. We chose several carbon supports with lower surface area (Table S4†) than commercial carbon black (EC600) to synthesize Ru/N-C. In this scenario, larger Ru NPs

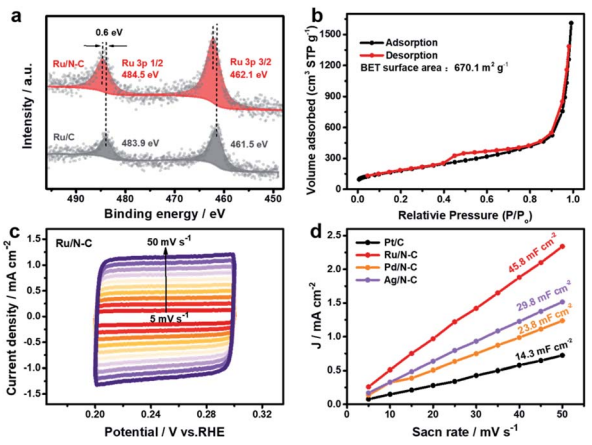

Fig. 5 (a) High-resolution XPS spectra of Ru 3p; (b) N_2 adsorption–desorption isotherm of Ru/N-C; (c) cyclic voltammetry curves of Ru/N-C at various scan rates from 5–50 mV s^{-1} in the region of 0.20–0.28 V *vs.* RHE; (d) C_{dl} comparison of Ru/N-C, commercial Pt/C, Pd/N-C and Ag/N-C.

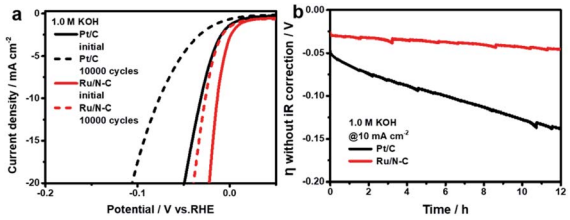

Fig. 6 (a) Polarization curves of Ru/N-C and commercial Pt/C initially and after 10 000 cycles, respectively, in 1.0 M KOH aqueous solution; (b) chronopotentiometry curves at 10 mA cm^{-2} in 1.0 M KOH solution.

(5.0–14.5 nm) were observed (Fig. S12 and S13†). EC600 by itself has a large surface area of 1270 m^2 g^{-1} and Ru/N-C has a surface area of 670.1 m^2 g^{-1} (Table S4† and Fig. 5b). The corresponding Ru/N-C exhibits the best HER activity in both alkaline and acidic electrolytes (Fig. S14†). Furthermore, the EC600 derived Ru/N-C has a larger double layered capacitance (C_{dl}) of 45.8 mF cm^{-2} at non-Faraday area than that of commercial Pt/C (Fig. 5c, d and S15†). This again suggests that the high surface area of EC600 is advantageous for the exposure of active sites.

The durability of Ru/N-C was studied by 10 000 times of potential cycling from 0.1 to −0.1 V (*vs.* RHE) at 100 mV s^{-1} in 1 M KOH aqueous solution. For comparison, commercial Pt/C was measured under the same conditions. The overpotential of Ru/N-C at 10 mA cm^{-2} only degrades by 13.5 mV (Fig. 6a), while commercial Pt/C negatively shifts 45 mV. This clearly exhibits that Ru/N-C is superior to that of commercial Pt/C. After durability test, Ru NPs are still homogeneously distributed on N-C without apparent size increase. While serious aggregation and particle size increase from 3.9 ± 0.8 to 9.1 ± 2.8 nm were observed for the case of commercial Pt/C (Fig. S16†).

Additionally, chronopotentiometry measurement shows that the overpotential of Ru/N-C at 10 mA cm^{-2} without *iR* correction increases by 16 mV over a period of 12 h (Fig. 6b) and particle size only increases from 2.2 ± 0.4 to 2.5 ± 0.5 nm (Fig. S17a and b†). In stark contrast, the overpotential increases by 89 mV and Pt NPs seriously agglomerate with an average size increase from 3.9 ± 0.8 to 9.8 ± 4.0 nm for commercial Pt/C (Fig. S17c and d†), which again evidences the superior durability of Ru/N-C. In 0.5 M H_2SO_4 aqueous solution, Ru/N-C has an excellent durability similar to that of commercial Pt/C (Fig. S18†). Again, the morphology of Ru/N-C after acidic durability test shows little change (Fig. S19†). We speculate that the nitrogen dopant may have tightly anchored the Ru NPs by coordination with Ru, thus preventing Ru NPs from migration and agglomeration.

Experimental

Material preparation

Ruthenium(III) chloride ($RuCl_3$, 35.0–38.0% Ru) was obtained from Shenyang Non-ferrous Metal Research Institute. Silver nitrate ($Ag(NO)_3$, >98%) was purchased from Tianjin Bodi Chemical Co., Ltd. Potassium tetrachloropalladate (K_2PdCl_4, EP) was purchased from Tianjin Fengchuan Chemical Reagent Technology Co., Ltd. Polyvinylpyrrolidone (PVP, average mol. wt. 40 000) was purchased from Sigma-Aldrich. Ethylene glycol (AR, 98%) was purchased from Shanghai Macklin Biochemical Co., Ltd. Multi-walled carbon nanotubes, short carboxyl multi-walled carbon nanotubes, short hydroxyl multi-walled carbon nanotubes and hydroxyl multi-walled carbon nanotubes were purchased from Chengdu Institute of Organic Chemistry, Chinese Academy of Sciences. Commercial Pt/C (20 wt%) was received from Johnson Matthey Chemical Co., Ltd. Nafion resin solution (5 wt%) was obtained from DuPont. Carbon black (Ketjenblack EC600 JD) was obtained from Akzo Nobel. Concentrated sulfuric acid (GR, 98%) was purchased from Jinzhou Gucheng Reagent Factory. Concentrated nitric acid (AR) was purchased from Tianjin Kemiou Chemical Reagent Co., Ltd. Potassium hydroxide (KOH, AR) was obtained from Sinopharm Chemical Reagent Co. Ltd.

Pretreatment of carbon black

In a round-bottomed flask, EC600 (3 g) was dispersed in 3 M nitric acid aqueous (300 mL) under mild sonication for at least 20 min for well dispersion. Then, the flask was placed in a water bath at 80 °C under stirring for 3 h of reflux. After cooling down to room temperature, the mixture was subjected to vacuum filtration with deionized water until the pH reaches to 7. Finally, the product was dried in an oven at 65 °C for 1 day.

Synthesis of highly dispersed Ru/N-C

Firstly, above treated carbon black (32 mg) and polyvinylpyrrolidone (PVP, average mol. wt. 40 000, 40 mg) were dispersed in ethylene glycol (EG, 25 °C, 4 mL) with the aid of 1 min of mild sonication and stirring. Next, ruthenium chloride ($RuCl_3$, 0.02 M in EG, 4 mL) was added under vigorous stirring, followed by 3 h of incubation at 180 °C in an oil bath. After cooling down to room temperature, the precipitates were collected by filtration under vacuum and washed with about 150 mL of deionized water. Next, the solids were dried in an oven at 65 °C for 1 day. After being ground, the solids were calcined in a H_2 (5 vol%)/Ar at a flow rate of 200 mL min^{-1}. Specifically, the solids were heat-treated from room temperature to 150 °C with a ramp rate of 5 °C min^{-1} and kept at 150 °C for 2 h. Finally, the temperature was further increased to 350 °C at 5 °C min^{-1} and kept at 350 °C for another 2 hours to attain Ru/N-C. For comparison, a series of pyrolysis temperature (250 °C, 450 °C, 550 °C, 650 °C, 750 °C) for the second heating was employed to synthesize other samples. And nitrogen doped multi-walled carbon nanotubes, short carboxyl multi-walled carbon nanotubes, short hydroxyl multi-walled carbon nanotubes and hydroxyl multi-walled carbon nanotubes were also employed for the synthesis of electrocatalysts under the same conditions except that the treated carbon black was replaced.

Synthesis of Pd/N-C and Ag/N-C

Ruthenium chloride was replaced by potassium tetrachloropalladate and silver nitrate for the synthesis of Pd/N-C and Ag/N-C, respectively, while holding all of the other synthetic parameters constant.

Synthesis of Ru/C, Pd/C, Ag/C

These electrocatalysts were synthesized by leaving out PVP while keeping all of the other synthetic parameters the same.

Characterizations

Transmission electron microscopy (TEM) was carried out on a Tecnai G2 F30 S-Twin. High-resolution transmission electron microscopy (HRTEM) and elemental mapping were operated on a JEM-F200. X-ray diffraction patterns (XRD) were collected on a Rigaku SmartLab 9 kW operating at 45 kV and 200 mA with Cu Kα radiation (λ = 1.5406 Å) with a Cu Kα radiation source (Rigaku, Japan). X-ray photoelectron spectroscopy (XPS) was collected on a ESCALAB XI^+ (Thermo Scientific) with monochromatized Al Kα (1486.6 eV) as the photon source. Surface area of samples was evaluated by nitrogen adsorption–desorption isotherms in combination of Brunauer–Emmett–Teller (BET) method on a Quantachrome Quadrasorb-SI Analyzer (Quantachrome, USA). Thermogravimetric analysis (TGA) was performed on a TA-Q600 in a temperature range from room temperature to 650 °C with a heating rate of 10 °C min^{-1} in dry air. ICP-OES (Optima 2000DV PerkinElmer) was used to analyze the composition of samples.

Electrochemical measurements

A CHI760D electrochemical workstation (Shanghai Chenhua Instruments Ltd.) and a three-electrode electrochemical cell were used to evaluate electrochemical reactions. A glassy carbon rotating disk electrode (RDE, 5 mm in diameter) coated with electrocatalysts was used as the working electrode (WE) with a carbon rod as the counter electrode. Hg/Hg_2SO_4 (saturated K_2SO_4) was chosen as the reference electrode (RE) in 0.5 M H_2SO_4 aqueous solution and Hg/HgO (1.0 M NaOH) was used as the RE in 1.0 M KOH aqueous solution. Typically,[40–42] 2 mg mL^{-1} electrocatalyst ink was prepared by dispersing certain amount of electrocatalyst in the mixture of water/ethanol/Nafion (5 wt%) at a volume ratio of 1 : 9 : 0.06 under 5 min of ultrasonication. RDE was polished with 5 μm and 30–50 nm alumina paste and then cleaned with ethanol and water. 20 μL of the ink was dropped onto the surface of RDE to reach an electrocatalyst loading of about 0.2 mg cm_{disk}^{-2}. Commercial Pt/C (20 wt%, Johnson Matthey) serves as a reference electrocatalyst. All of the RDE tests were performed in N_2-saturated 0.5 M H_2SO_4 or 1.0 M KOH aqueous solution at 25 °C. HER polarization curves were obtained by linear sweep voltammetry (LSV) with a negative sweep rate of 5 mV s^{-1} and a rotation rate of 1600 rpm. Durability test was operated by potential cycling from −0.1 to 0.1 V (*vs.* RHE) at 100 mV s^{-1}. Internal resistance (*iR*) was assessed by *iR* compensation on CHI760D and all of the data were corrected for 85% *iR* potential drop.

TOF calculation

The TOF per metal site of Ru/N-C and commercial Pt/C toward HER is calculated according to following equation:[39]

$$\mathrm{TOF} = \frac{\text{total number of hydrogen turnovers/geometric area } (\mathrm{cm^2})}{\text{number of active sites/geometric area } (\mathrm{cm^2})} \quad (1)$$

The total number of hydrogen turnovers was calculated from the current density using formula (2):

$$\begin{aligned}\text{Number of hydrogens} &= j\ (\mathrm{mA\ cm^{-2}})\ 1\ \left(\mathrm{C\ s^{-1}}(10^3\ \mathrm{mA})^{-1}\right) \\ &\times \left(1\ \mathrm{mol\ e^-}\ (96485.3C)^{-1}\right) \times \left(\frac{1\ \mathrm{mol\ H_2}}{2\ \mathrm{mol\ e^-}}\right) \\ &\times \left(\frac{6.022\times10^{23}\ \mathrm{molecules\ H_2}}{1\ \mathrm{mol\ H_2}}\right) \\ &= 3.12\times10^{15}\ \mathrm{H_2\ per\ s\ per\ cm^2} \end{aligned} \quad (2)$$

The number of Ru metal sites was determined from the ICP-OES measurement (12.1 wt%).

Accordingly, the active site density based on total Ru is calculated according to eqn (3):

$$\begin{aligned}\text{Active site density} &= \frac{12.1}{100}\times\left(0.2\ \mathrm{mg\ cm^{-2}}\right)\times\left(\frac{1\ \mathrm{mmol}}{101.07\ \mathrm{mg}}\right) \\ &\times 6.022\times10^{20}\ \text{sites per mmol} \\ &= 1.44\times10^{17}\ \mathrm{Ru\ sites\ per\ cm^2} \end{aligned} \quad (3)$$

Conclusions

In summary, we report the synthesis of highly dispersed Ru NPs (2.2 ± 0.4 nm) on nitrogen doped carbon by chemical reduction of $RuCl_3$ on carbon in the presence of PVP in combination with subsequent pyrolysis. Ru/N-C exhibits an excellent overpotential of 13.5 and 18.5 mV at 10 mA cm^{-2} in 1.0 M KOH and 0.5 M H_2SO_4 aqueous, respectively, much better than and comparable to that of commercial Pt/C (38.0 and 10.0 mV). The exceptional HER activity arises from the high surface area of ultrafine Ru NPs and an appropriate Ru electronic state tuned by nitrogen dopant. Furthermore, Ru/N-C demonstrates an excellent durability in both alkaline and acidic condition relative to commercial Pt/C.

Author contributions

Gen Li: conceptualization, data curation, investigation, writing – original draft. Rui Gao: resources, writing – review & editing. Zhongyu Qiu: writing – review & editing. Wei Liu: writing – review & editing. Yujiang Song: supervision, project administration, writing – review & editing. All authors have discussed and given approval to the final version of the manuscript.

Conflicts of interest

There are no conflicts to declare.

Acknowledgements

This study was supported by the Talent project of Revitalizing Liaoning (Grant No. XLYC2002067), the Science & Technology Innovation Funds of Dalian (Grant No. 2020JJ25CY003), the Key Research and Development Plan of Liaoning Province in 2020 (Grant No. 2020JH2/10100025), and the Fundamental Research Funds for the Central Universities (Grant No. DUT19ZD208 and DUT20ZD208).

Notes and references

1 Z. Zhang, P. Li, Q. Wang, Q. Feng, Y. Tao, J. Xu, C. Jiang, X. Lu, J. Fan, M. Gu, H. Li and H. Wang, *J. Mater. Chem. A*, 2019, **7**, 2780–2786.
2 J. Mahmood, F. Li, S. Jung, M. S. Okyay, I. Ahmad, S. Kim, N. Park, H. Y. Jeong and J. Baek, *Nat. Nanotechnol.*, 2017, **12**, 441–446.
3 D. H. Kweon, M. S. Okyay, S. Kim, J. Jeon, H. Noh, N. Park, J. Mahmood and J. Baek, *Nat. Commun.*, 2020, **11**, 1278.
4 Q. Song, X. Qiao, L. Liu, Z. Xue, C. Huang and T. Wang, *Chem. Commun.*, 2019, **55**, 965–968.
5 B. Guo, X. Zhang, J. Xie, Y. Shan, R. Fan, W. Yu, M. Li, D. Liu, Y. Chai and B. Dong, *Int. J. Hydrogen Energy*, 2021, **46**, 7964–7973.
6 D. Wang, M. Gong, H. Chou, C. Pan, H. Chen, Y. Wu, M. Lin, M. Guan, J. Yang, C. Chen, Y. Wang, B. Hwang, C. Chen and H. Dai, *J. Am. Chem. Soc.*, 2015, **137**, 1587–1592.
7 X. Long, G. Li, Z. Wang, H. Zhu, T. Zhang, S. Xiao, W. Guo and S. Yang, *J. Am. Chem. Soc.*, 2015, **137**, 11900–11903.
8 Y. Shi, Y. Zhou, D. Yang, W. Xu, C. Wang, F. Wang, J. Xu, X. Xia and H. Chen, *J. Am. Chem. Soc.*, 2017, **139**, 15479–15485.
9 S. Piontek, C. Andronescu, A. Zaichenko, B. Konkena, K. Junge Puring, B. Marler, H. Antoni, I. Sinev, M. Muhler, D. Mollenhauer, B. Roldan Cuenya, W. Schuhmann and U. Apfel, *ACS Catal.*, 2018, **8**, 987–996.
10 X. Meng, L. Yu, C. Ma, B. Nan, R. Si, Y. Tu, J. Deng, D. Deng and X. Bao, *Nano Energy*, 2019, **61**, 611–616.
11 J. Yang, A. R. Mohmad, Y. Wang, R. Fullon, X. Song, F. Zhao, I. Bozkurt, M. Augustin, E. J. G. Santos, H. S. Shin, W. Zhang, D. Voiry, H. Y. Jeong and M. Chhowalla, *Nat. Mater.*, 2019, **18**, 1309–1314.
12 J. Yin, Q. Fan, Y. Li, F. Cheng, P. Zhou, P. Xi and S. Sun, *J. Am. Chem. Soc.*, 2016, **138**, 14546–14549.
13 Z. Kou, T. Wang, H. Wu, L. Zheng, S. Mu, Z. Pan, Z. Lyu, W. Zang, S. J. Pennycook and J. Wang, *Small*, 2019, **15**, 1900248.
14 W. Liu, X. Wang, F. Wang, K. Du, Z. Zhang, Y. Guo, H. Yin and D. Wang, *Nat. Commun.*, 2021, **12**, 6776.
15 G. Zeng, T. A. Pham, S. Vanka, G. Liu, C. Song, J. K. Cooper, Z. Mi, T. Ogitsu and F. M. Toma, *Nat. Mater.*, 2021, **20**, 1130–1135.
16 L. Tian, X. Yan and X. Chen, *ACS Catal.*, 2016, **6**, 5441–5448.
17 D. Y. Chung, S. W. Jun, G. Yoon, H. Kim, J. M. Yoo, K. Lee, T. Kim, H. Shin, A. K. Sinha, S. G. Kwon, K. Kang, T. Hyeon and Y. Sung, *J. Am. Chem. Soc.*, 2017, **139**, 6669–6674.
18 X. Yu, Z. Yu, X. Zhang, Y. Zheng, Y. Duan, Q. Gao, R. Wu, B. Sun, M. Gao, G. Wang and S. Yu, *J. Am. Chem. Soc.*, 2019, **141**, 7537–7543.
19 X. F. Lu, L. Yu and X. W. D. Lou, *Sci. Adv.*, 2019, **5**, v6009.
20 J. Yu, Y. Guo, S. She, S. Miao, M. Ni, W. Zhou, M. Liu and Z. Shao, *Adv. Mater.*, 2018, **30**, 1800047.
21 Z. Pu, X. Ya, I. S. Amiinu, Z. Tu, X. Liu, W. Li and S. Mu, *J. Mater. Chem. A*, 2016, **4**, 15327–15332.
22 T. Sun, S. Zhang, L. Xu, D. Wang and Y. Li, *Chem. Commun.*, 2018, **54**, 12101–12104.
23 B. Song, K. Li, Y. Yin, T. Wu, L. Dang, M. Cabán-Acevedo, J. Han, T. Gao, X. Wang, Z. Zhang, J. R. Schmidt, P. Xu and S. Jin, *ACS Catal.*, 2017, **7**, 8549–8557.
24 Z. Wu, X. Li, W. Liu, Y. Zhong, Q. Gan, X. Li and H. Wang, *ACS Catal.*, 2017, **7**, 4026–4032.
25 X. Tan, S. Geng, Y. Ji, Q. Shao, T. Zhu, P. Wang, Y. Li and X. Huang, *Adv. Mater.*, 2020, **32**, 2002857.
26 P. Zhang, H. Xue and N. Suen, *Chem. Commun.*, 2019, **55**, 14393–14544.
27 X. Cao, R. Fan, J. Zhou, C. Chen, S. Xu, S. Zou, W. Dong, X. Su, S. Ju and M. Shen, *Chem. Commun.*, 2022, **58**, 1569–1572.
28 Q. Yao, B. Huang, N. Zhang, M. Sun, Q. Shao and X. Huang, *Angew. Chem., Int. Ed.*, 2019, **58**, 13983–13988.
29 T. Qiu, Z. Liang, W. Guo, S. Gao, C. Qu, H. Tabassum, H. Zhang, B. Zhu, R. Zou and Y. Shao-Horn, *Nano Energy*, 2019, **58**, 1–10.
30 Y. Xiao, W. Liu, Z. Zhang and J. Liu, *J. Colloid Interface Sci.*, 2020, **571**, 205–212.
31 X. Que, T. Lin, S. Li, X. Chen, C. Hu, Y. Wang, M. Shi, J. Peng, J. Li, J. Ma and M. Zhai, *Appl. Surf. Sci.*, 2021, **541**, 148345.
32 B. Lu, L. Guo, F. Wu, Y. Peng, J. E. Lu, T. J. Smart, N. Wang, Y. Z. Finfrock, D. Morris, P. Zhang, N. Li, P. Gao, Y. Ping and S. Chen, *Nat. Commun.*, 2019, **10**, 631.
33 Z. Chen, J. Lu, Y. Ai, Y. Ji, T. Adschiri and L. Wan, *ACS Appl. Mater. Interfaces*, 2016, **8**, 35132–35137.
34 R. Ye, Y. Liu, Z. Peng, T. Wang, A. S. Jalilov, B. I. Yakobson, S. Wei and J. M. Tour, *ACS Appl. Mater. Interfaces*, 2017, **9**, 3785–3791.
35 D. Hyung Kweon, I. Jeon and J. Baek, *Advanced Energy and Sustainability Research*, 2021, **2**, 2100019.
36 Y. Li, L. A. Zhang, Y. Qin, F. Chu, Y. Kong, Y. Tao, Y. Li, Y. Bu, D. Ding and M. Liu, *ACS Catal.*, 2018, **8**, 5714–5720.
37 S. Anantharaj and S. Noda, *Small*, 2019, **16**, 1905779.
38 Q. Song, X. Qiao, L. Liu, Z. Xue, C. Huang and T. Wang, *Chem. Commun.*, 2019, **55**, 965–968.
39 J. N. Tiwari, S. Sultan, C. W. Myung, T. Yoon, N. Li, M. Ha, A. M. Harzandi, H. J. Park, D. Y. Kim, S. S. Chandrasekaran, W. G. Lee, V. Vij, H. Kang, T. J. Shin, H. S. Shin, G. Lee, Z. Lee and K. S. Kim, *Nat. Energy*, 2018, **3**, 773–782.
40 Y. Lv, H. Liu, J. Li, J. Chen and Y. Song, *J. Electroanal. Chem.*, 2020, **870**, 114172.
41 H. Han, Y. Wang, Y. Zhang, Y. Cong, J. Qin, R. Gao, C. Chai and Y. Song, *Acta Physica Sinica -Chinese Edition*, 2020, **37**, 2008017.
42 Y. Lv, H. Liu, J. Qin, R. Gao, Y. Zhang, Y. Xie, J. Li and Y. Song, *Prog. Nat. Sci.: Mater. Int.*, 2020, **30**, 832–838.